

Computer Modeling Chemical Vapor Infiltration of SiC Composites

Yaochan Zhu¹, Eckart Schnack¹, Al Mahmudur Rahman¹

Abstract: A novel multiphase field model is formulated to simulate the complex microstructure evolution during chemical vapor infiltration (CVI) process, which is widely used technique to produce SiC matrix composites reinforced by SiC fibers in ceramic engineer. The model consists of a set of nonlinear partial differential equations by coupling Ginzburg-Landau type phase field equations with mass/heat balance equations as well as modified Navier-Stokes equations. The microstructure evolution of preferential codeposition of Si, SiC and C under high ratio of H₂ to MTS is simulated. The simulation is in good agreement with experiments result. The potential risk of blockage of the premature pores is predicted. By investigating the effect of gas flow and chemical reaction on concentration field of MTS, it is found that the gas flow is in favor of the homogeneous distribution of MTS while this distribution is mainly dominated by chemical reaction. Meanwhile, the effect of thermal gradient on CVI process is investigated.

Keywords: Composites, chemical vapor infiltration, modeling.

1 Introduction

Silicon carbide fibers reinforced silicon carbide ceramic matrix composite (SiC/SiC) is of excellent thermo-physical and mechanical properties at elevated temperature. It has been considered as one of most important candidate for structural components in high-temperature application, such as for high-performance turbines, aerospace and nuclear fusion reactors [Y. Xu, X. Yan (2010)]. Fig. 1 shows the micrograph of SiC/SiC material and the typical fracture surface (Image courtesy of MT Aerospace AG). Among different fabrication processes of SiC/SiC, chemical vapor infiltration (CVI) appears to be the method of choice because CVI spares the strong but relatively fragile fibers from damaging thermal, mechanical and chemical degradation. During CVI process, the woven fibers preform is heated and selected gaseous reactants are infiltrated through its internal substrate pore space via diffusion and/or

¹ Karlsruhe Institute of Technology, Germany. Email: yao.zhu@kit.edu

forced viscous flow. As infiltration proceeds, there occurs the densification process on fibers. It's an extension of chemical vapor deposition (CVD) process in which coating occurs on the internal surface of fibers preform. By pyrolysis of Methyltrichlorosilane (MTS), the deposition of SiC with excess Si, SiC with excess C and stoichiometric SiC can be realized. Extensive experiments research have been

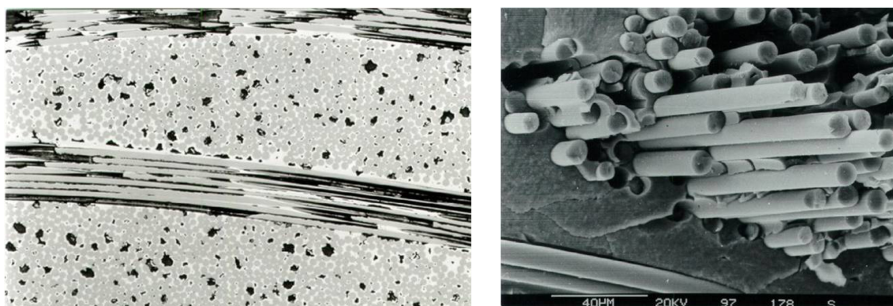


Figure 1: Micrograph (left) of SiC/SiC composites and the typical fracture surface (right)

devoted to investigate the influence of the infiltration conditions on deposition product, such as temperature, pressure and the ratio of H_2 to MTS. In order to explore the influence of the infiltration conditions on CVI process, an increasing demand of understanding the process details (transport, fluid flow, reaction mechanism) was required. This leads to the application of simulation techniques to study CVI process. Up to now, to build a CVI model with the interaction among heterogeneous pores evolution, transport, gas fluid flow and chemical reaction being accounted is still a great challenge. The success of phase field method in microstructure simulation provides us a potential solution.

2 Multiphase-field model of the chemical vapor infiltration

2.1 CVI thermodynamics and kinetics

During SiC CVI process, MTS as precursor and Hydrogen(H_2) as carrier gas are pumped into the reactor. For thermal decomposition of MTS, the reduced mechanism is adopted which allows a detailed thermodynamics description. In the following, based on the work by [W. G. Zhang, G. K. Huttinger (2001); Allendorf M. D. Allendorf and T. H. Osterheld (1995); E. Fitzer and D. Kehr (1976)], a model of both homogeneous gas phase chemistry and heterogeneous surface chemistry is presented. Here CH_3 and C_2 species are assumed to be the carbon sources, while

SiCl₃ and HSiCl₃ are assumed to be the silicon sources for the deposition of C, Si and SiC.

Dissociation reaction of MTS:



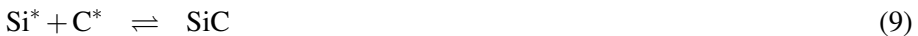
C-bearing species:



Si-bearing species:



Formation of the depositions (* indicates the surface adsorption):



The above chemical reactions are governed by thermodynamics and kinetics. The thermodynamics defines the driving force which indicates the potential direction that the reaction will proceed. The kinetics defines the transport process and subsequently determines the rate-control step during chemical vapor deposition. Both of these two aspects of information should be reflected in CVI model. The free energy changing for a reaction is defined as:

$$\Delta G_r = \sum z^i \Delta G_{f,i}^0 + RT \ln Q \quad (10)$$

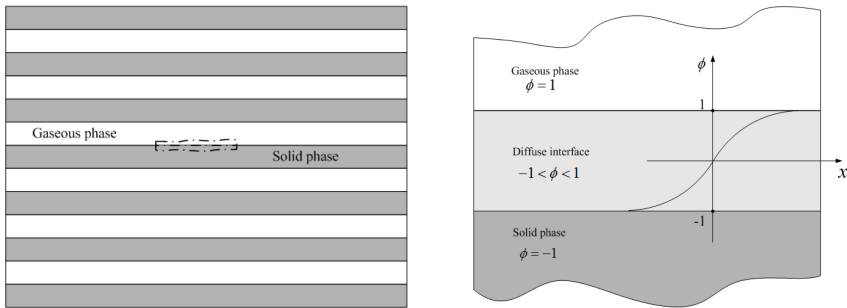
where z^i is the stoichiometric coefficient of species i in reaction (negative for reactants, positive for products). R is the ideal gas constant. Q is the reaction quotient which is related to the activity and partial pressure of species i ; $G_{f,i}^0$ is the standard free energy of formation of species i at temperature T and 1 atm as:

$$\Delta G_{f,i}^0 = \Delta H_i + T \Delta S_i \quad (11)$$

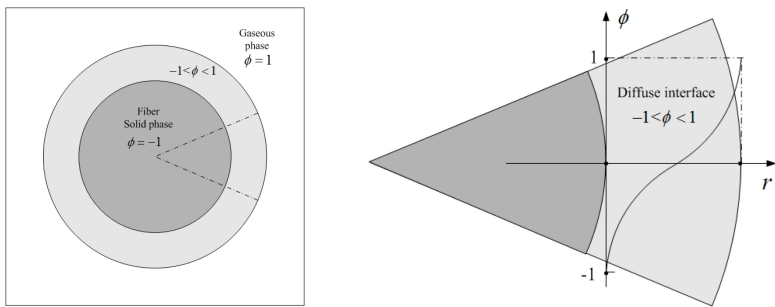
where the enthalpies H and the entropies S can be calculated based on JANAF thermochemical tables [M. W. Chase (1998)]. The thermodynamics properties of individual substances can refer to [L. V. Gurvich, I. V. Veyts, C. B. Alcock (1989)].

2.2 Phase-field equations

Phase-field method is used to predict the microstructures evolution during the CVI process in this work. As shown in Fig. 2, the gas-solid interface is implicitly denoted by the spatially diffusive phase field order parameter ϕ instead of sharp interface. Therefore the spatio-temporal behavior of phase field order parameter reproduces the deposited SiC microstructure evolution. Multiphase field order parameters are adopted for the codeposition of SiC, Si and C under specific CVI processing conditions. The existence of bulk phase i is represented $\phi_i = 1, i = 1..N$ (N is the number of phases), otherwise 0 in the rest phases, and $0 < \phi_i < 1$ in interfaces. Here we define that ϕ_1 denotes the multi-component gaseous phase and ϕ_2, ϕ_3, ϕ_4 denote silicon, silicon carbide, carbon respectively.



(a) Scheme in the fiber axis



(b) Scheme in the fiber vertical direction

Figure 2: Schematic illustration of the definition of the phase-field parameter ϕ

The Ginzburg-Landau type of system free energy can be expressed as:

$$F = \int_{\Omega} \sum_{j>i=1}^N \sum_{i=1}^N \left[-\frac{\varepsilon_{ij}^2}{2} \nabla \phi_i \nabla \phi_j + W_{ij} \phi_i \phi_j + f_e + \lambda_L \left(\sum_{i=1}^N \phi_i - 1 \right) \right] d\Omega \quad (12)$$

here the gradient energy coefficient ε_{ij} and the height of the energy barrier W_{ij} together contribute the interfacial properties. The Lagrange multiplier λ_L is introduced to account for the sum of phase field in the system being conserved. The first term with the gradient of phase fields accounts for energy penalty for the formation of interfaces. The second term is the energy barrier to prevent phase transition occurring randomly. f_e is the chemical free energy density of local bulk phases, which can be interpolated by:

$$f_e = \sum_i^N \phi_i \Delta G_r^i \quad (13)$$

Based upon this above thermodynamical description, the interface evolution can be accounted by Geinzburg-Landau phase field equation.

$$\frac{\partial \phi_i}{\partial t} = \sum_{j \neq i}^n -\frac{2s_{ij}M_{ij}}{n} \left[\sum_{j \neq i}^n \left[\frac{\varepsilon_{ij}^2}{2} (\nabla^2 \phi_j - \nabla^2 \phi_i) + W_{ij}(\phi_j - \phi_i) \right] + \Delta G_i - \Delta G_j \right] \quad (14)$$

where s_{ij} is the identification function [I. Steinbach, F. Pezzolla, B. Nestler, M. Seesselberg, R. Prieler, G. J. Schmitz, J. Rezende (1996)] to locate interface between phase i and j . M_{ij} is the interface mobility. n is the number of phases coexisting in a given point. In the following, mass and heat transport as well as gas flow will be coupled with phase field order parameters.

2.3 Mass transport

The mass transport of the species in CVI process can be stated in the compact form of a time-dependent convection-diffusion problem:

$$\partial_t c_i = -\phi_1 (\mathbf{u} \cdot \nabla) c_i + \nabla \cdot [D \nabla c_i] + r_i^{\text{eff}}, i \in \{\text{gaseous species}\} \quad (15)$$

where c_i is the molar concentration of gaseous species i . $i \in \{\text{gaseous species}\}$ indicates that the diffusion of each species in solid phases is disregarded due to its low diffusivity. \mathbf{u} is the velocity vector. D is the diffusivity which is a function of effective binary diffusion coefficient D_i in gas (γ_j being the molar fraction of component j , $D_{i,j}$ being the binary diffusion coefficient of species i and j):

$$D = \sum_i^N \phi_i D_i, \quad D_i = 1 / \sum_{j \neq i} \frac{\gamma_j}{D_{i,j}} \quad (16)$$

The effective chemical reaction rate r_i^{eff} is assumed as a combination of the homogeneous gaseous reaction and heterogeneous surface reaction:

$$r_i^{\text{eff}} = \phi_1 r_i^{\text{hom}} + (1 - \phi_1) \delta(\phi_i) r_i^{\text{het}} \quad (17)$$

with r_i^{hom} as the homogeneous reaction rate (gaseous reaction rate) of species i and r_i^{het} as the heterogeneous reaction rate (surface reaction rate) of species i . $\delta(\phi_i)$ is a step function [E. Schnack, F. W. Wang and A. J. Li (2010)].

2.4 Fluid motion

In this work, solid phases are assumed to be rigid and stationary. Following modified Navier-Stokes equations is employed to describe the gas flow.

$$\nabla \cdot (\phi_1 \mathbf{u}) = 0 \quad (18)$$

$$\begin{aligned} \rho \frac{\partial (\phi_1 \mathbf{u})}{\partial t} = & -\rho (\phi_1 \mathbf{u} \cdot \nabla) \mathbf{u} + \phi_1 \nabla \cdot (-p) \mathbf{I} \\ & + \eta \nabla \cdot [\nabla (\phi_1 \mathbf{u}) + (\nabla (\phi_1 \mathbf{u}))^T] + B \eta (\phi_1^2 (1 - \phi_1) \mathbf{u}) \end{aligned} \quad (19)$$

here \mathbf{u} is the velocity. ρ is the density (the same density assumed for different gaseous species for simplicity), and η is the viscosity. \mathbf{I} is the unit metric and T is the inversion sign. B is the parameter depending on the gradient energy coefficient ε [C. Beckermann, H. J. Dipers, I. Steinbach, A. Karma, and X. Tong (1999)]. The last term in Equ.(19) is the force term, which is chosen such that the no-slip condition can be accurately reproduced regardless of the diffusive interface thickness.

2.5 Heat transport

Isothermal CVI (ICVI) causes the preferential deposition near the surface of the substrate, leaving the interior of the preform poorly densified. The thermal gradient CVI (TGCVI) allows better densification of the matrix through preventing early closing the surface pores. During TGCVI, the preform is kept at a temperature gradient and the vapor precursor diffuses through the preform from the cool side to the hot regions. From modeling point of view, only the imposed boundary conditions are different for ICVI and TGCVI. The uniform formulation of heat balance can be applied for both solid and gas phase in the whole domain except that heat convection should be included in gas phase as a fluid. The following heat convection and conduction equation is used.

$$\rho C_p \frac{\partial T}{\partial t} + \nabla \cdot (-k \nabla T) + \rho C_p \phi_1 \mathbf{u} \cdot \nabla T - Q = 0 \quad (20)$$

here T is temperature and \mathbf{u} is the velocity. ρ is the density, C_p is the heat capacity at constant pressure and k is thermal conductivity. Q is a heat source or a heat sink by chemical reaction. For simplicity, Q is assumed to be zero. The interpolation of convective term by ϕ_1 is to ensure that the convection is limited in gas phase. The density, heat capacity and heat capacity of the gaseous phase and solid phase differ greatly. Therefore the following interpolation is applied in the model:

$$\rho = \sum_i \phi_i \rho_i, \quad C_p = \sum_i \phi_i C_p^i, \quad k = \sum_i \phi_i k_i \quad (21)$$

where $i = 1$ denotes the multicomponent gaseous phase, therefore the corresponding density, heat capacity and heat capacity of gas phase are averaged ones. $i = 2, 3, 4$ denote silicon, silicon carbide and carbon, respectively.

3 Simulation result and discussion

The formulation of our multiphase field model consists of Eq. 14, Eq. 15, Eq. 18, Eq. 19 and Eq. 20. With appropriated initial and boundary conditions, the model will be implemented on the geometric model as shown in Fig. 3 for unidirectional fibre-reinforced composite. For three dimensional case, the one-fiber or the multi-fibers model can be used. Due to the symmetry along the radial section of the fiber, this three dimensional model often can be reduced to a 2D model. The numerical

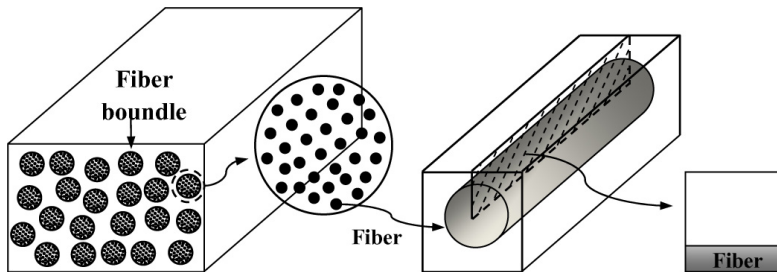


Figure 3: Schematic illustrations of unidirectional fiber-reinforced substrates

discretization for the model consists of two parts: implicit Euler finite difference approximation for temporal discretization and Galerkin weighted residual method for spatial discretization. The numerical simulation are performed by using COMSOL Multiphysics based on distributed parallelization calculation.

Considering that isothermal chemical vapor infiltration (ICVI) process is the most important and basic approach for fabricating SiC/SiC, the simulation will focused

on ICVI (temperature being constant) first and then extended to the case considering the effect of thermal gradient. The model parameters are listed in Tab. 1:

Fig. 4 shows the microstructure evolution and corresponding MTS concentration

Table 1: Parameters related to model

Parameter	Value	Parameter	Value
$\epsilon_{ij} (\text{Jm}^{-1})^{1/2}$	$5.8e-4$	$W_{ij} (\text{Jm}^{-1})$	$1.32e7$
$p (\text{Pa})$	$1.01325e5$	$M_{ij} (\text{ms}^{-1})$	$2.09e-7$
$T (\text{K})$	1123	$u_x (\text{ms}^{-1})$	$3e-2$
$\rho_g (\text{Kg} \cdot \text{m}^{-3})$	0.067	$\rho_s (\text{Kg} \cdot \text{m}^{-3})$	3200.0
$D_{\text{CH}_3\text{SiCl}_3, \text{H}_2} (\text{m}^2 \cdot \text{s}^{-1})$	$7.26e-4$	$D_{\text{HCl}, \text{H}_2} (\text{m}^2 \cdot \text{s}^{-1})$	$1.47e-3$
γ_{H_2}	0.9	γ_{MTS}	0.1
$l_{2D} (\text{m})$	$2e-5$	$l_{3D} (\text{m})$	$1e-5$
$\eta_s (\text{Pa} \cdot \text{s})$	2.6	$\eta_g (\text{Pa} \cdot \text{s})$	$2.62e-5$

field during SiC deposition. It can be found that the growth of solid phase nearby precursor inlet side is much faster than that nearby outlet side, which implies that the risk of blockage of the premature pores increases. Also we can find that the C (graphite) phase tends to be eliminated by SiC phase because of its overgrowth. This is accordant with experiments [F. Loumagne (1995); G. D. Papasouliotis and S. V. Sotirchos (1994)] that only codeposition of Si(s) and SiC(s) exists while C (graphite) phase is absent in under the high ratios of H₂ to MTS (>104) as in this study. As time pass by, concentration of MTS nearby the inlet side much higher than that of the rest, and this distribution favors the growth of the solid phase nearby inlet side. The concentration of MTS at section A and B at different moment is shown in Fig. 5. The step increasing in the curves along section B indicates the location of gas/solid interface, with left part in solid phase and the right part in gas phase. It shows that as time goes on, the c_{MTS} along both these two sections decreases; the gradient decreasing of c_{MTS} along section A is obvious which is mainly caused chemical reaction as being explained later; there barely exists change of c_{MTS} along section B because the effect of diffusion is weak comparing to that caused by chemical reaction.

By changing the reaction diffusion equation, the effect of fluid flow and chemical reaction on c_{MTS} distribution is investigated. Three cases are set up: **a)** only diffusion is considered; **b)** constant fluid flow is considered in mass transport equation based on case a; **c)** chemical reaction in mass transport equation is considered based on case a. Simulation shows that the fluid flow in case b changes MTS concentration field as in case a and tends to reduce the concentration gradient as shown

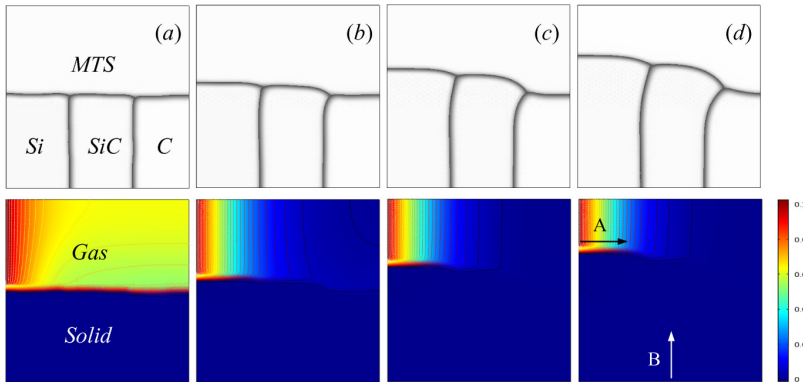


Figure 4: Phase field evolution and gas composition distribution at scaled time: a) $t=0.1$; b) $t=0.5$; c) $t=1$; d) $t=1.5$

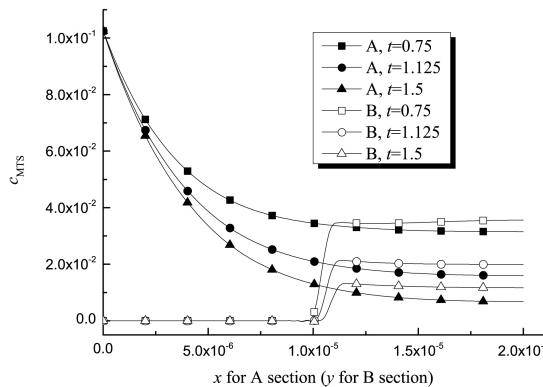


Figure 5: Time dependent c_{MTS} at section A and B

in the Fig. 6. This homogenization of MTS is in favour of the even deposition to reduce the potential pore blockages which cause the porosity in matrix. After chemical reaction is introduced into the diffusion equation as in case c the concentration nearby inlet side is quickly decreased to small value nearby outlet side of the reactor, which indicates that MTS is highly reactive and is prone to decomposing. This inhomogeneous MTS distribution impedes the even deposition to achieve highly densified production.

Under appreciate infiltration conditions, the single phase SiC is deposited. Fig. 3 shows the growth of multi SiC grains with different initial seed size. It's found

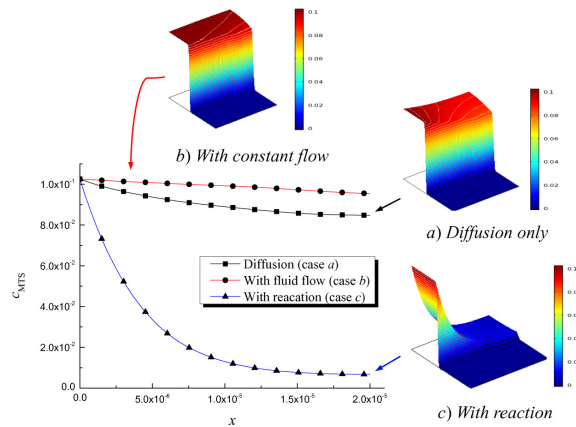


Figure 6: The effect of fluid and chemical reaction on c_{MnS}

that as deposition proceeds, the SiC grains with small size tend to be eliminated by those surrounding grains by the competitive growth. The coarse SiC grains in final microstructure is accordant with experimental results which show that the tiny grain on the deposition surface are gradually coarsen. Thermal gradient CVI

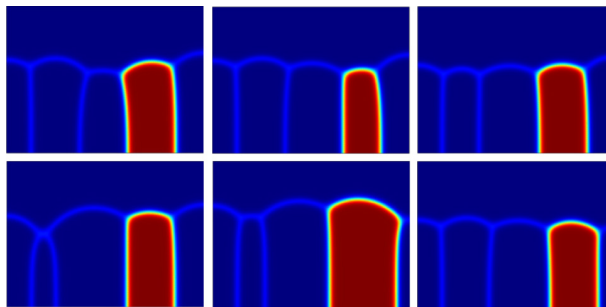


Figure 7: SiC deposited as grains

is a hot-wall technique. As show in Fig. 8, a faster SiC deposition nearby outlet side (hot region) occurs compared with deposition nearby inlet side (cold region). In this figure, the marked line is the solid-gas interface between deposited SiC matrix (downside area) on fiber and gaseous phase (upside area). Therefore the temperature gradient helps to prevent the formation of pore blockage nearby inlet side in which the fiber is exposed to precursor gases in the low temperature region

first. Due to significant difference in thermal conductivities of gaseous phase and solid phase (i. e. fiber+matrix), the temperature distribution shows a transition area along the deposition surface. In addition, the temperature distribution at gaseous phase will be affected by gas fluid. Comparing figure as shown in the Fig. 8(a) and Fig. 8(b), it could be found that the faster the gas from cold inlet side to hot wall, the steeper of the temperature gradient near by outlet side.

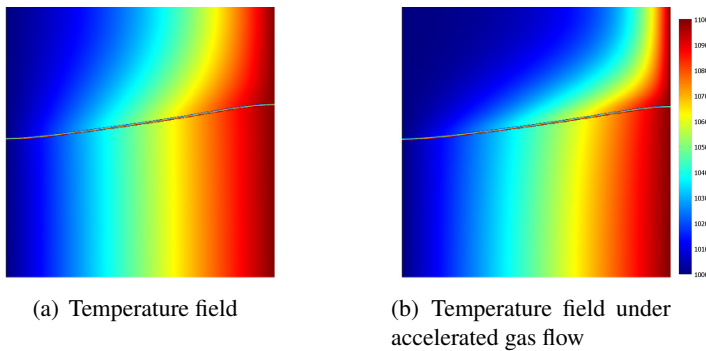


Figure 8: Thermal gradient of TGCVI

4 Conclusion

The multiphase-field model is developed in this research to predict the microstructures evolution during the CVI process of SiC. The model consists of the Ginzburg-Landau phase field equations, mass/heat transport equation and the modified Navier-stokes equations. By this model the multi solid phase codeposition behavior is described. The microstructure evolution of the preferential codeposition of Si(s), SiC(s) is reproduced with kinetic inhibition of C(graphite) phase which is in accordant with experimental research. Meanwhile the potential risk of blockage of the premature pores during ICVI process is predicted. Simulations show that the concentration of MTS is homogenized by fluid flow which is in favour of the even deposition while this concentration field is mainly dominated by the chemical reaction. The multi SiC grains deposition simulation reproduce the competitive growth mechanism during the coarse process. Grains with small size tend to be eliminated and coarsen grain left in final microstructure. The simulation found that thermal gradient helps to prevent the formation of pore blockage and the gradient at gaseous phase nearby outlet side will be enhanced by accelerated gas flow.

Acknowledgement: The financial support by the German Research Foundation (DFG Schn 245/31) and KTRG fund (CATECH/KTRG/GERMANY/1325) by College of Aviation Technology (Bangladesh) is gratefully acknowledged.

References

- C. Beckermann, H. J. Dipers, I. Steinbach, A. Karma, and X. Tong** (1999): Modeling melt convection in phase-field simulations of solidification. *J. Comput. Phys*, vol. 154, pp. 468–159.
- E. Fitzer and D. Kehr** (1976): Carbon, carbide and silicide coatings. *Thin Solid Films*, vol. 39, pp. 55–57.
- E. Schnack, F. W. Wang and A. J. Li** (2010): Phase-field model for the chemical vapour infiltration of silicon carbide. *Journal of the electrochemical society*, vol. 157, pp. 377–386.
- F. Loumagne, F. Langlais, R. N.** (1995): Experimental kinetic study of the chemical vapour deposition of sic-based ceramics from $\text{ch}_3\text{sicl}_3/\text{h}_2$ gas precursor. *J Cryst growth*, vol. 155, pp. 198–204.
- G. D. Pappasoulotis and S. V. Sotirchos** (1994): On the homogeneous chemistry of the thermal decomposition of methyltrichlorosilane. *Journal of the Electrochemical Society*, vol. 141, pp. 1599–1611.
- I. Steinbach, F. Pezzolla, B. Nestler, M. Seesselberg, R. Prieler, G. J. Schmitz, J. Rezende** (1996): A phase field concept for multiphase systems. *Physic D*, vol. 94, pp. 135–117.
- L. V. Gurvich, I. V. Veyts, C. B. Alcock** (1989): *Thermodynamic Properties of Individual Substances*. Hemisphere publishing.
- M. D. Allendorf and T. H. Osterheld** (1995): Modeling the gas-phase chemistry of silicon carbide formation. In B. M. Gallosi, W. Y. Lee and M. A. Pickering(Ed): *Chemical vapor deposition of refractory metals and ceramics Iii*, pp. 39–44. World Science Publishers.
- M. W. Chase** (1998): Nist-janaf thermochemical talbles. *J. Phys. Chem. Ref. Data*, vol. 9.
- W. G. Zhang, G. K. Huttinger** (2001): Chemical vapor deposition of sic from methyltrichlorosilane partii: Composition of the gas phase and the deposit. *Adv. Mater. CVD*, vol. 7, pp. 173–181.
- Y. Xu, X. Yan** (2010): *Chemical Vapour Deposition: An integrated engineering design for advanced materials*. Springer.